Check for updates

ADVANCED FUNCTIONAL MATERIALS
www.afm-journal.de

Activated Immune System Determines In Vivo Anti-Tumor Effect of Phototherapy by Inhibiting Cancer-Associated Fibroblasts

Mengchao Ding, Haoyu Chen, Carlos F. Guimarães, Rui L. Reis, Lijuan Wu, Fenglan Zhang, Yaqian Lv, Tianyi Wang, Qihui Zhou, Jinsheng Shi,* and Xiaoying Kong**

Immune activation has been widely recognized to promote anti-tumor effects in vivo. However, in previous anti-tumor studies of combined photo/immunotherapy, the tumor apoptosis pathway is widely regarded as an independent process, which led to an incomplete understanding of the anti-tumor mechanisms of the immune system during phototherapy. Herein, the decisive role of immune activation for the anti-tumor effect of phototherapy and its specific mechanism, are investigated by preparing a melanin@chlorin e6@hyaluronic acid and oxidized *Bletilla striata* polysaccharide@NO-donor (MCH-OBN) nanoplatform, which integrated significant immune activation by phototherapy. The comparison of anti-tumor effects between wild-type mice and immunodeficient mice showed that effective phototherapy provided by the MCH-OBN can not independently kill tumor cells in vivo, as it significantly depends on the immune activation. Furthermore, the activated immune system is demonstrated to destroy the tumor cell "barrier protection" by inhibiting the growth of cancer-associated fibroblasts (CAFs), thereby ensuring the damage of heat, reactive oxygen species (ROS), and other components of phototherapy to the tumor. Thus, this work reveals for the first time the biological consequences of immune activation that determine the anti-tumor effect of phototherapy by regulating CAF proliferation, which is of great significance for optimizing anti-tumor clinical treatments through phototherapy.

1. Introduction

Solid tumors generally have an immunosuppressed tumor microenvironment (TME), which is infiltrated by a large number of immune-resistant tumor-associated fibroblasts, leading the majority of tumors to persist in such an immune "cold" state.[1–4] In the past decade, the anti-tumor research of phototherapy has confirmed that thermal ablation[5] and free radicals such as reactive oxygen species (ROS)[6] and reactive nitrogen species (RNS)[7] provided by photothermal therapy (PTT)[8–10] and photodynamic therapy (PDT)[11] can promote the secretion of tumor-associated antigens (TAAs), oxidative damage of cells, and the upregulation of immunogenic cell death (ICD) and cellular pyroptosis.[12] Phototherapy therefore could induce the transition of the tumor from a "cold" to a "hot" immune state, thus enhancing the sensitivity of the tumor to immunotherapy.[13,14] Thus, the effective combination of phototherapy and immunotherapy is expected to achieve a synergistic amplification of the anti-tumor therapeutic effect. In the past, the research on the relationship between phototherapy and the immune system mostly focused on the activation of the immune system by heat and free radicals.[6,15] Therefore, the direct involvement of the activated immune system in the attack of tumor cells by thermal ablation and active small molecules in phototherapy still requires further evidence to be confirmed. The activated immune system has still not been proven to regulate the clinical

M. Ding, H. Chen, F. Zhang, T. Wang, X. Kong
College of Chemistry and Pharmaceutical Sciences
Qingdao Agricultural University
Qingdao 266109, China
E-mail: xykong@qau.edu.cn
M. Ding
School of Biomedical Sciences and Engineering
South China University of Technology
Guangzhou 510650, China
C. F. Guimarães, R. L. Reis
3B's Research Group-Research Institute on Biomaterials
Biodegradables and Biomimetics
University of Minho
Headquarters of the European Institute of Excellence on Tissue
Engineering and Regenerative Medicine
Parque de Ciência e Tecnologia
Zona Industrial da Gandra – Avepark
Guimarães 4805-017, Portugal
C. F. Guimarães, R. L. Reis
ICVS/3B's – Portuguese Government Associate Laboratory
University of Minho
Guimarães 4800-058, Portugal

The ORCID identification number(s) for the author(s) of this article can be found under https://doi.org/10.1002/adfm.202315551

DOI: 10.1002/adfm.202315551

 © 2024 Wiley-VCH GmbH

anti-tumor effect of phototherapy, in turn indicating that the anti-tumor pathways of phototherapy and the activated immune system were considered to be independent of each other in the present research. To uncover the anti-tumor consequences of the immune system during phototherapy, it is necessary to explore whether the activated immune system is directly involved in the anti-tumor treatment process of phototherapy from a TME-corresponding perspective.

Numerous studies have shown that anti-tumor chemotherapy requires the involvement of the immune system, and once immunogenic cell ICD is induced, the ratio of cytotoxic T lymphocyte (CTL)/Treg in the tumor increases,[16,17] thus providing a more satisfactory prognosis for patients. At present, relevant data mainly focuses on breast/colon cancer research.[18,19] In addition, the results of animal tumor-bearing experiments (including transplanted and primary tumors induced by chemicals) showed that the chemotherapy effect was statistically different between wild-type and immunodeficient mice groups.[20] These studies have fully proven that the therapeutic effect of chemotherapy drugs is not only due to the cytotoxic effect of drugs but also closely dependent on the activation of the immune system, establishing a research paradigm for the relationship between specific anti-tumor techniques and the immune system. In addition, the infiltration of immune cells, heat ablation, and diffusion of active small molecules all showed a correlation with the spatial structure of the tumor, suggesting the synergistic effect of immune activation and phototherapy against tumor cells in space. Therefore, inspired by the above studies on the dependence of anti-tumor effects of chemotherapy drugs on the immune system as well as the synergistic speculation, one can hope to explore the immune dependence of anti-tumor effects from phototherapy (including photothermal and photodynamic therapies). This is of great clinical significance for reexamining the unsatisfactory anti-tumor effect of phototherapy in the specific treatment process in the past and further improving its synergistic treatment strategy.

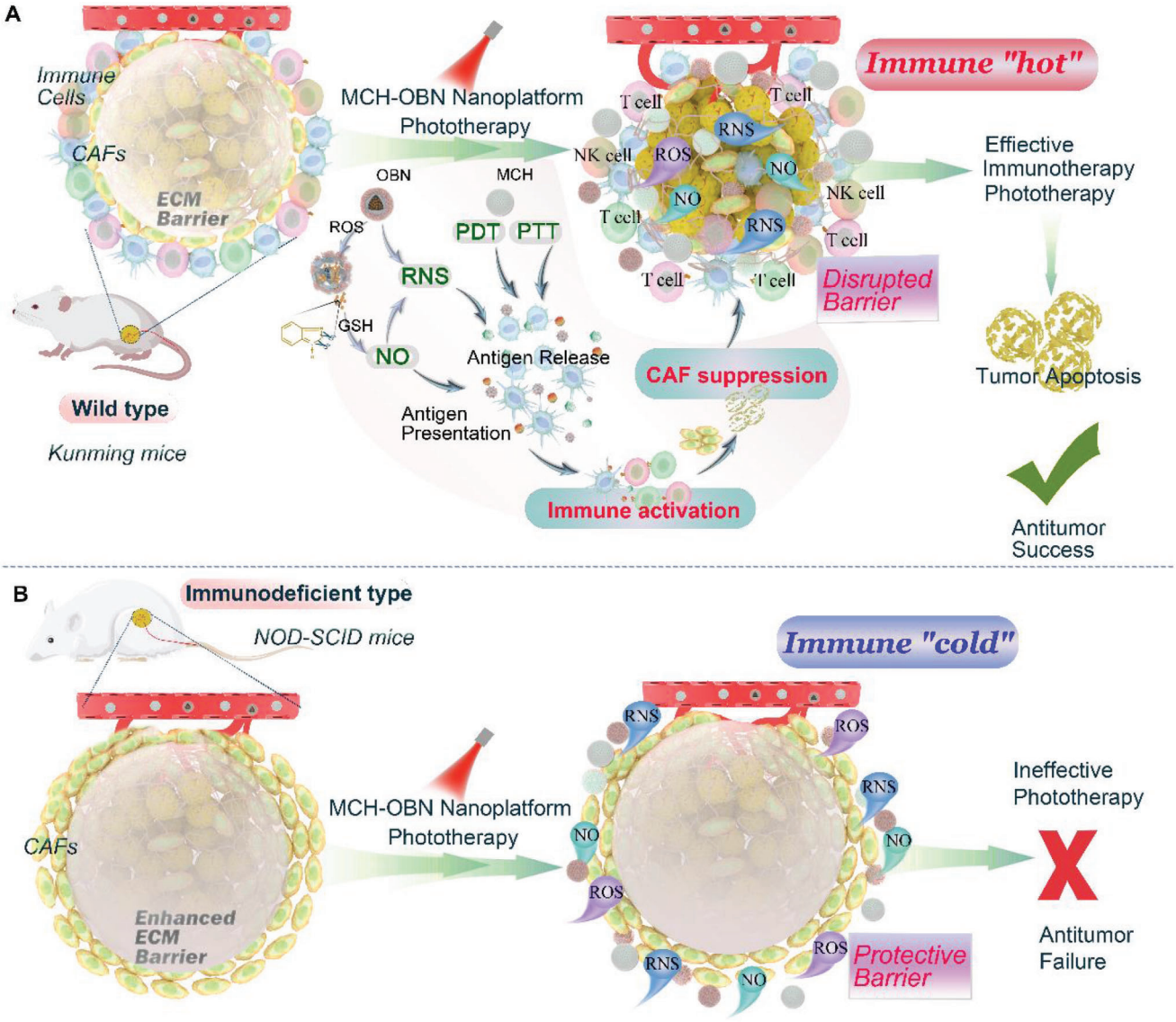
On the premise of the above hypothesis, it is necessary to explore the specific mechanism by which the activated immune system regulates the anti-tumor effect of phototherapy. Inspired by the high sensitivity of both the immune system and phototherapy to tumor steric hindrance, it is further hypothesized that this dependence is related to the tumor "protective barrier" – provided by the cancer-associated fibroblasts (CAFs). In tumor tissues that are under immunosuppression, the high proportion of CAFs in the tumor microenvironment leads to the further absence of anti-tumor immune members, such as dendritic cells (DCs) and cytotoxic T cells, which brings great challenges for the anti-tumor phototherapy and immune activation.[21–23] In immunologically "cold" solid tumors, the proportion of CAFs with high expression of TGF-β1 and α-SMA is as high as 50%.[24] Moreover, CAFs secrete collagen-rich extracellular matrix and improve the autophagy ability of tumor cells, which can downregulate the infiltration of immune cells and the presentation of DCs, thereby forming a dense physical barrier surrounding the tumor tissue, which then more easily resists the attack of the immune system.[25–27] Recent in vitro 3D models have also shown that the simple presence of fibroblasts in the vicinity of cancer cells can confer a degree of protection against chemotherapeutic drugs.[28] In addition, the physical isolation provided by the extracellular matrix secreted by CAFs may also play a crucial role in reducing the killing effect of PTT and PDT on tumor cells due to the limitation of the heat conduction distance and the faster quenching of free radicals such as ROS in phototherapy.[29–31] Studies have confirmed that fibroblast activation protein (FAP)-specific chimeric antigen receptor (CAR) T cells can eliminate most FAP+ cells, including CAFs, and inhibit the production of tumor stroma,[32] which suggests that members of anti-tumor immunity can cause efficient anti-tumor effects by inhibiting the proliferation and ECM secretion from CAFs. Therefore, there is an antagonistic or competitive relationship between the anti-tumor immune members and CAFs at the tumor site. Inspired by the above studies, we hypothesized that the infiltration and activation of anti-tumor immune members at the tumor site may play a crucial role in the final anti-tumor effect of phototherapy by inhibiting the proliferation of CAFs. CAFs, as the important members in the TME, protect tumor cells from phototherapy damage in the "cold" immune state. Instead, in the "hot" immune state, the activated immune system may ensure that phototherapy can break through the "protective layer" by inhibiting CAFs, thus ensuring the high efficiency of phototherapy in killing tumor cells.

Herein, a nanoplatform consisting of melanin@chlorin e6@hyaluronic acid nanoparticles (MCH NPs) and oxidized *Bletilla striata* polysaccharide@NO donor (OBN) microcapsules were prepared for combining phototherapy and NO/reactive nitrogen therapy. MCH-OBN nanoplatform aimed at achieving significant immune activation and tumor apoptosis, thus providing a good condition for subsequent research on the relationship between phototherapy and immune activation. As a vasodilator, NO can effectively improve the penetration of nanoparticles at the tumor site, thus enhancing the anti-tumor feasibility of the phototherapy carrier in this study.[33–35] In addition, the production of active RNS with the co-participation of ROS and NO further sensitized the immune activation at the tumor site. Therefore, the assistance of OBN microcapsules to MCH NPs is of great significance for the development of this work. By analyzing the breast cancer treatment efficacy in wild-type and immunodeficient mice, the tumor-killing ability of the phototherapy provided by the MCH-OBN nanoplatform between wild-type mice and immunodeficient mice was further compared to determine the decisive role of the activated immune

L. Wu
Innovation Platform of Marine Drug Screening & Evaluation
Qingdao National Laboratory for Marine Science and Technology
Qingdao 266237, China
Y. Lv
School of Veterinary Medicine
Qingdao Agricultural University
Qingdao 266109, China
Q. Zhou
Qingdao Key Laboratory of Materials for Tissue Repair and Rehabilitation
School of Rehabilitation Sciences and Engineering
University of Health and Rehabilitation Sciences
Qingdao 266113, China
E-mail: qihuizhou@uor.edu.cn
J. Shi
Department of Public Course Teaching
University of Health and Rehabilitation Sciences
Qingdao 266113, China
E-mail: shijinsheng@uor.edu.cn

© 2024 Wiley-VCH GmbH

16163028, 0, Downloaded from https://onlinelibrary.wiley.com/doi/10.1002/adfm.202315551 by Universidade Do Minho, Wiley Online Library on [26/03/2024]. See the Terms and Conditions (https://onlinelibrary.wiley.com/terms-and-conditions) on Wiley Online Library for rules of use; OA articles are governed by the applicable Creative Commons License



Scheme 1. Schematic diagram of the anti-tumor effect of the MCH-OBN phototherapy nanoplatform under different immune states. MCH-OBN phototherapy nanoplatform was prepared to achieve significant DC cell and cytotoxic T cell activation and tumor cell apoptosis, providing a good condition for subsequent research on the relationship between phototherapy and immune activation. CAFs, as the important members in the TME, protect tumor cells from phototherapy damage in the immune "cold" state. While in the immune "hot" state, the activated immune system may ensure that phototherapy can break through the "protective barrier" by inhibiting CAFs, thus ensuring the high efficiency of phototherapy in killing tumor cells.

system in the anti-tumor effect of phototherapy (**Scheme 1**). On this basis, the specific mechanisms of CAFs in protecting tumors from damage of phototherapy were explored, and the activated immune system was confirmed to ensure the effectiveness of phototherapy by inhibiting the proliferation of CAFs. In conclusion, this work provides a comprehensive analysis of the relationship between the immune system and the effects of phototherapy. This study further outlines the specific mechanism of immune system participation in the anti-tumor treatment of phototherapy from the perspective of CAF regulation, which is of great significance for the developing combining application of phototherapy, immune therapy, and CAF-targeting therapy.

2. Results and Discussion

2.1. Characterization of MCH-OBN Nanoplatform

MNP@Ce6@HA (MCH) NPs and Oxi-BSP@NO donor (OBN) microcapsules were prepared by chemical bonding and self-assembly, which is shown in **Figures 1**a,b. TEM and dynamic laser scattering exhibited the successful preparation of MCH NPs and OBN microcapsules with 208 ± 5.8 and 199 ± 2.1 nm, respectively. The change of zeta potential (Figure S1, Supporting Information) reflected the preparation process of MCH NPs and OBN microcapsules. In addition, the PBAP (ROS response group) and BSP showed a successful covalent connection, which was

© 2024 Wiley-VCH GmbH

16163028, 0, Downloaded from https://onlinelibrary.wiley.com/doi/10.1002/adfm.202315551 by Universidade Do Minho, Wiley Online Library on [26/03/2024]. See the Terms and Conditions (https://onlinelibrary.wiley.com/terms-and-conditions) on Wiley Online Library for rules of use; OA articles are governed by the applicable Creative Commons License

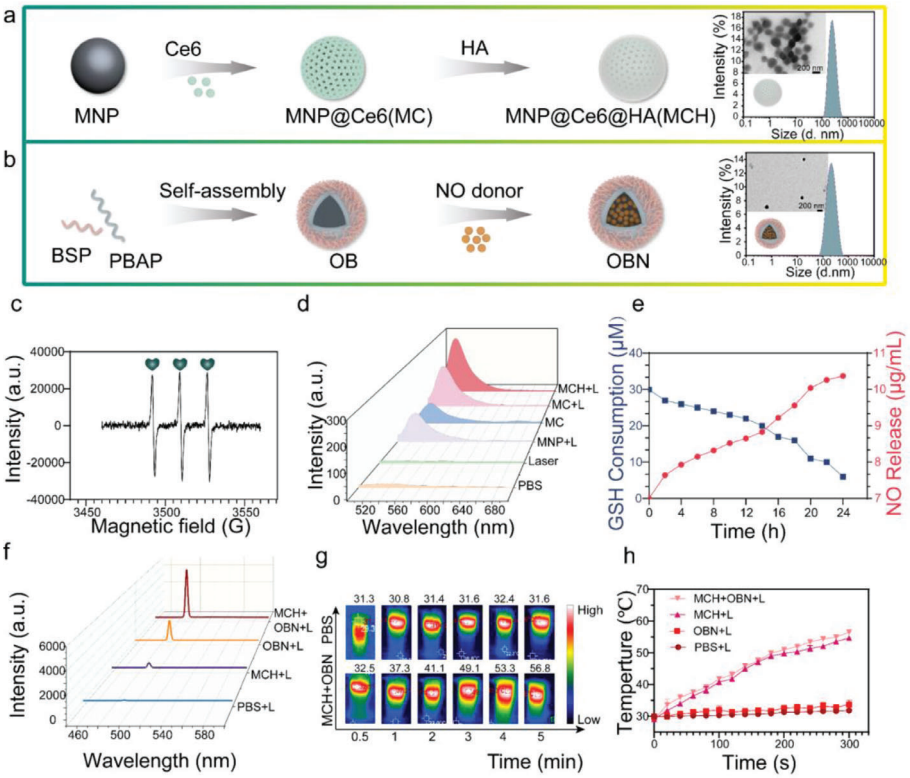


Figure 1. Characterization of MCH-OBN nanoplatform. a,b) Synthetic scheme of MCH NPs and OBN microcapsules attached with hydrodynamic diameters and TEM images; c) EPR spectra of MCH NPs with 808 nm laser (1 W cm^{-2}, 5 min); d) Fluorescence intensity of ROS in 4T1 cells treated with PBS, Ce6 (1 mg mL^{-1}), MH (1 mg mL^{-1}), and MCH (1 mg mL^{-1}) under 808 nm laser irradiation (1 W cm^{-2}, 5 min); e) Release of NO and consumption of GSH by the NO donor; f) Fluorescence intensity of RNS in 4T1 cells treated with PBS, MCH (1 mg mL^{-1}), OBN (1 mg mL^{-1}), and MCH + OBN (1 mg mL^{-1}) under 808 nm laser irradiation (1 W cm^{-2}, 5 min); g,h) Infrared thermal images and temperature curves under NIR irradiation (808 nm, 1 W cm^{-2}, 5 min).

manifested by the appearance of cpharacteristic peaks at 1750 cm^{-1} in the OB and OBN FTIR spectra (C = O vibration). And the specific peaks at 1500 cm^{-1} of benzofuroxan (NO donor) in the OBN spectrum demonstrated successful loading of NO donor (Figure S2a, Supporting Information). Moreover, Ce6 was also successfully connected with MNP, which was verified by 890 and 930 cm^{-1} peaks (C-N vibration) in FTIR spectra of MCH (Figure S2b, Supporting Information).

Several of our group have previously confirmed that MCH NPs were not only excellent tumor photothermal materials and immunomodulators but also can realize ROS production under near-infrared irradiation (808 nm) without the participation of up-conversion materials,[36] where loading capacity (LC) and encapsulation efficiency (EE) of Ce6 can reach 2.6% and 10.4%. This work proved that MCH NPs can be used as a phototherapy carrier with both PTT and PDT functions under near-infrared excitation. According to electron paramagnetic resonance (EPR) (Figure 1c), the obvious 1:1:1 signal proved the generation of singlet oxygen ($^1O_2$) by MCH NPs, which was verified by Figure S3, Supporting Information and Figure 1d. Furthermore, ROS could react with PBAP and induce the OBN microcapsules to rupture and release benzofuroxan, which was the NO donor and the LC and EE were 7.8% and 13.5%. As indicated in Figure S5, Supporting Information, the release of benzofuroxan must be assisted with the participation of H_2O_2, and a more significant benzofuroxan release was observed under 10 mM H_2O_2 with the participation of MCH under NIR irradiation, suggesting that the rupture of OBN microcapsules and subsequent release of NO donors could be accelerated by ROS produced from MCH NPs. The released NO donor could react with the high concentration of glutathione in the tumor microenvironment to release NO. With the help of the standard curves of NO and GSH (Figure S6, Supporting Information), NO formation and GSH consumption were detected under the improvement of MCH NPs and OBN microcapsules (Figure 1e).

NO and ROS could further generate peroxynitrite anion ($ONOO^-$) and other reactive RNS, which feature higher stability, longer lifetime (10–20 s), and more persistent anti-tumor performance than ROS.[37] Among all the groups, MCH exhibited the strongest ROS generation ability (Figure 1d), and the MCH + OBN group showed the strongest RNS production ability (Figure 1f). Although mild PTT is increasingly adopted in anti-tumor therapy to alleviate the immune microenvironment, high-temperature PTT (50–60 °C) still has important clinical significance in tumor thermal ablation treatment.[38] In order to better simulate the immune state after clinical tumor thermal ablation, high temperature (50–60 °C) was selected as the condition for anti-tumor photothermal therapy in this study. As displayed in Figure S7a,b, Supporting Information, the optimal PTT condition of MCH + OBN nanoplatform was determined (808 nm, 1 W,

© 2024 Wiley-VCH GmbH

16163028, 0, Downloaded from https://onlinelibrary.wiley.com/doi/10.1002/adfm.202315551 by Universidade Do Minho, Wiley Online Library on [26/03/2024]. See the Terms and Conditions (https://onlinelibrary.wiley.com/terms-and-conditions) on Wiley Online Library for rules of use; OA articles are governed by the applicable Creative Commons License

1 mg mL^{-1}) and the photothermal conversion cycling of MCH NPs was stable. Furthermore, under irradiation of NIR (808 nm, 1 W) after 5 min, 1 mg mL^{-1} MCH-OBN could promote the temperature of PBS solution to be over 50 °C, which achieved the ideal temperature for tumor ablation (Figure 1g,h, and Figure S8, Supporting Information). Taken together, the MCH-OBN nanoplatform was successfully prepared and proved to exhibit satisfactory PTT/PDT properties and NO/RNS production ability, which ensured the high permeability of the nanoparticles in tumor tissues and the effect of phototherapy.

2.2. Cellular Uptake and Intracellular ROS/RNS Attack of MCH-OBN Nanoplatform

Successfully prepared MCH NPs and OBN microcapsules need to reach the tumor tissue at the same time, and then enter the tumor cells through endocytosis. As exhibited in **Figure 2**a, MCH NPs targeted and internalized through specific binding by HA to 4T1 cells which highly expresses the CD44 receptor.[39–41] Meanwhile, OBN microcapsules were passively endocytosed into cells after being injected in situ at the tumor site. Co-localization of MCH NPs and OBN microcapsules in tumor cells is a prerequisite for the generation of intracellular ROS, NO, and RNS. Subsequently, the localization of the NPs was observed through confocal laser scanning microscopy (CLSM) after 3 h of incubation of the cells with FITC-labeled MCH and RH123-labeled OBN (Figure 2b), which displayed that both MCH and OBN entered tumor cells by endocytosis. What is more, the accumulation of MCH NPs at the tumor site was observed through photothermal imaging (Figures S9 and S10, Supporting Information). Notably, the temperature at the tumor site can reach its highest at 6 h after administration, which indicates the peak time of tumor accumulation of MCH NPs. Based on these results, the in situ administration time for OBN material was determined to be 6 h post-MCH administration, which endowed the co-localization of MCH and OBN at the tumor site. Subsequently, CLSM images showed weak ROS content in the MCH/OBN group while significantly higher ROS content in the MCH + OBN + Laser group (Figure 2c,d), indicating the reliance of ROS production on the presence of laser. Higher ROS also promoted the generation of higher RNS in the MCH + OBN + Laser group (Figure 2e,f). Compared to the control group, the cell membranes in MCH + OBN + Laser group were blurred and oxidized (Figure 2g), and the mitochondrial membrane potential (MMP) of cells treated by MCH + OBN + Laser was the lowest (Figure 2h,i), indicating severe oxidative damage as well as serious leakage of Cytochrome c caused by high concentration of ROS and RNS. Therefore, the cooperation of high concentrations of ROS and RNS resulted in severe destruction of cellular oxidation balance, leading to significant oxidative damage to cell membranes and mitochondria.

2.3. In Vitro Killing Effect on 4T1 Cells and Immune Activation

With the assistance of NO and RNS, phototherapy could cause severe oxidative damage to the tumor cell membrane, DNA, and mitochondria.[42,43] As displayed in **Figure 3**a,b, tumor cells suffered severe apoptosis with the treatment of MCH + OBN + Laser. However, the MCH NPs utilized in this study possess specific targeting capabilities due to their coating of HA. These nanoparticles can bind specifically to CD44 on the surface of tumor cells and enter them via endocytosis, which allows for the specific delivery of ROS to effectively damage tumor cells. Subsequently, the damaged tumor cells release antigenic factors or cell fragments, which are presented by antigen-presenting cells, ultimately leading to the activation of CD4+/CD8+ T cells. In this process, ROS was generated in a controlled environment and at a precise location. Notably, the damage inflicted by these nanoparticles on non-specific T cells is minimal, which is indirectly supported by the safety profile of these nanoparticles on normal cells as demonstrated in Figure 3c. Many studies have confirmed that thermal ablation, ROS, and RNS can improve the immunosuppressive state of the tumor site by upregulating the ICD of tumor cells, so as to sensitize tumor immunotherapy.[44,45] Antigen-presenting cells (APC) such as DCs often fail to recognize and present the antigen due to the immunosuppressive environment established by other tumor-promoting immune members and the hiding of antigen signals by tumor cells, resulting in tumor immune escape.[46–48] In this work, after severe cellular damage caused by MCH + OBN + Laser, upregulated CRT and downregulated HMGB1 expression (Figure 3d–g), which are representative signals of ICD,[49,50] induced maturation of DCs and antigen-presenting, which was verified by the transwell system composed by DCs and 4T1 cells (Figure 3h). Compared with the control group and other treatments, MCH + OBN + Laser treatment on 4T1 cells could induce a significant maturation of CD86+CD80+ DCs (Figure 3i). Major histocompatibility complex-II (MHC-II), could process these antigens into peptides to form the peptide-MHC-II complex when DCs are activated, thus targeting T cell receptors for antigen presentation.[51,52] As exhibited in Figure 3j, the percentage of expressed MHC-II of DCs treated with MCH + OBN + Laser increased from 14.3% to 35.1%, also implying significant upregulation of maturation and antigen presentation ability of DCs by MCH-OBN nanoplatform. Taking the above results into consideration, satisfactory in vitro anti-tumor effect and DC activation effect have been achieved by MCH-OBN nanoplatform, providing an excellent phototherapy carrier for the successful development of subsequent immune-dependent studies in this work.

2.4. In Vivo Anti-Tumor Therapy and Immune Activation in Wild-Type Kunming Mice

In this work, wild-type Kunming mice bearing 4T1 tumor cells were first used as an animal model to detect the anti-tumor effect of MCH-OBN nanoplatform under normal immune state (**Figure 4**a). Firstly, in order to detect the safety of the MCH-OBN treatment in mice, hematoxylin and eosin (H&E) staining of major organs (heart, liver, spleen, lung, and kidney) was performed (Figure S11, Supporting Information), which revealed no significant injury or inflammatory lesions after treatment. Meanwhile, hematological parameters and serum indicators were detected and found to be within the normal range (Figure S12, Supporting Information), including white blood cells (WBC), red blood cells (RBC), hemoglobin (HGB), and alkaline phosphatase (ALP), alanine aminotransferase (ALT), and blood urea nitrogen

© 2024 Wiley-VCH GmbH

16163028, 0, Downloaded from https://onlinelibrary.wiley.com/doi/10.1002/adfm.202315551 by Universidade Do Minho, Wiley Online Library on [26/03/2024]. See the Terms and Conditions (https://onlinelibrary.wiley.com/terms-and-conditions) on Wiley Online Library for rules of use; OA articles are governed by the applicable Creative Commons License

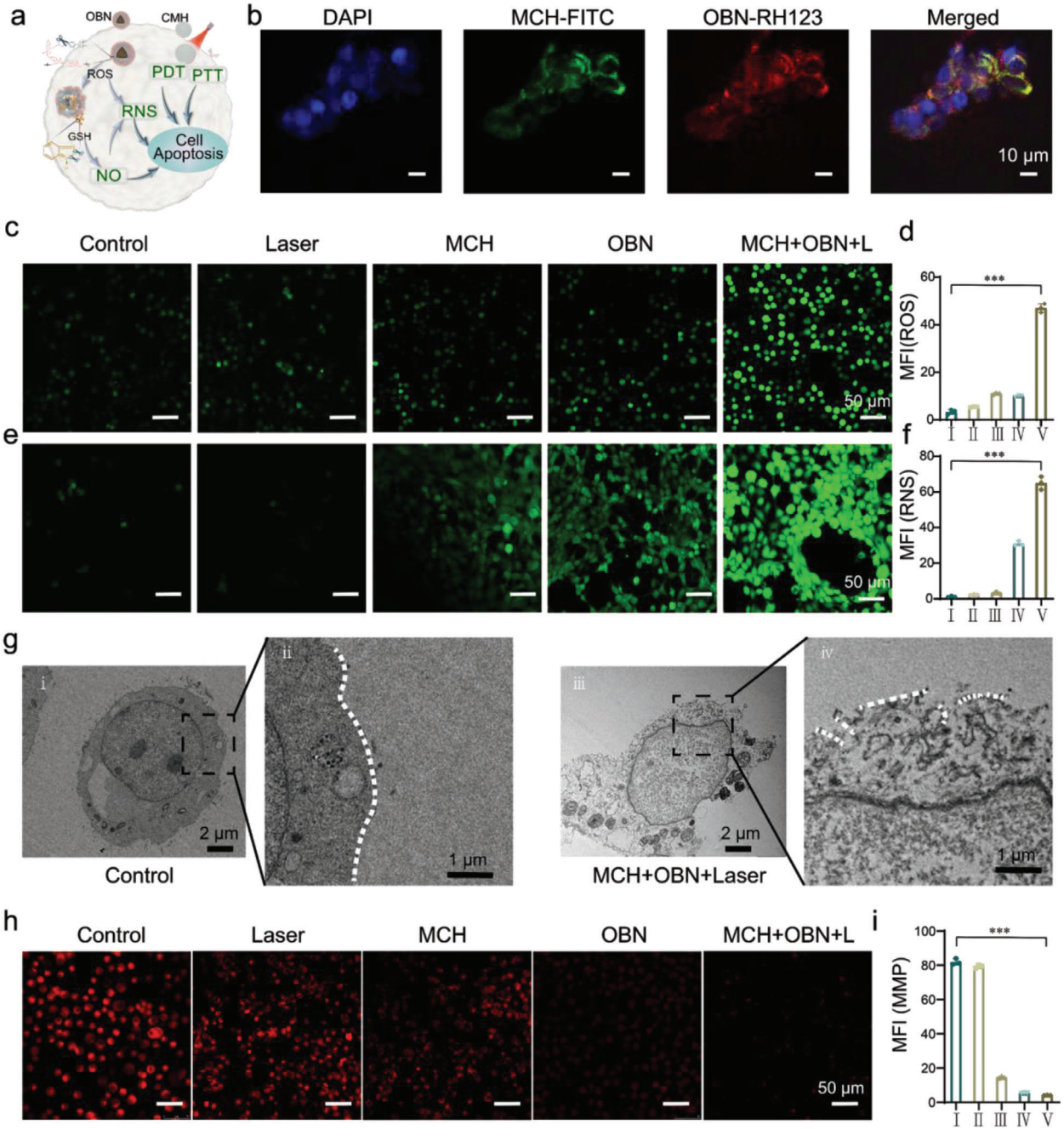


Figure 2. Cellular uptake of nanoparticles and detection of ROS/RNS and related cellular damage. a) Schematic diagram of MCH and OBN entering 4T1 cells; b) CLSM images of intracellular co-location of MCH and OBN; c–f) CLSM images and relative quantitative analysis of mean fluorescence intensity (MFI) of c,d) ROS and e,f) RNS produced by 4T1 cells after different treatments (scale bar: 50 μm); g) Bio-TEM of the cell membrane after different treatments. (ii) and (iv) are the enlarged images of (i) and (iii). h,i) CLSM images and relative quantitative analysis of MFI of Mito Tracker Red CMXRos fluorescence after different treatments (scale bar: 50 μm). *I–V*: Control, Laser, MCH + Laser, OBN + Laser, MCH + OBN + Laser. Data were presented as mean ± SD ($n = 3$), $^{**}p < 0.01$, $^{***}p < 0.001$.

(BUN). Furthermore, no significant weight loss was found in all groups during the treatment (Figures S13 and S14, Supporting Information), all of this evidence indicated acceptable biosafety of MCH-OBN nanoplatform. After treatment with MCH-OBN nanoplatform, the tumor growth was significantly inhibited (Figure 4b,c, and Figures S15 and S17, Supporting Information), and the survival rate was effectively improved (Figure 4d). H&E staining and terminal deoxynucleotidyl transferase dUTP nick end labeling (TUNEL) assay showed significant shrinkage and apoptosis of 4T1 tumor cells by treatment of MCH-OBN nanoplatform (Figure 4e), which was designed to kill tumor cells through cell membrane oxidation, DNA damage, mitochondrial

© 2024 Wiley-VCH GmbH

16163028, 0, Downloaded from https://onlinelibrary.wiley.com/doi/10.1002/adfm.202315551 by Universidade Do Minho, Wiley Online Library on [26/03/2024]. See the Terms and Conditions (https://onlinelibrary.wiley.com/terms-and-conditions) on Wiley Online Library for rules of use; OA articles are governed by the applicable Creative Commons License

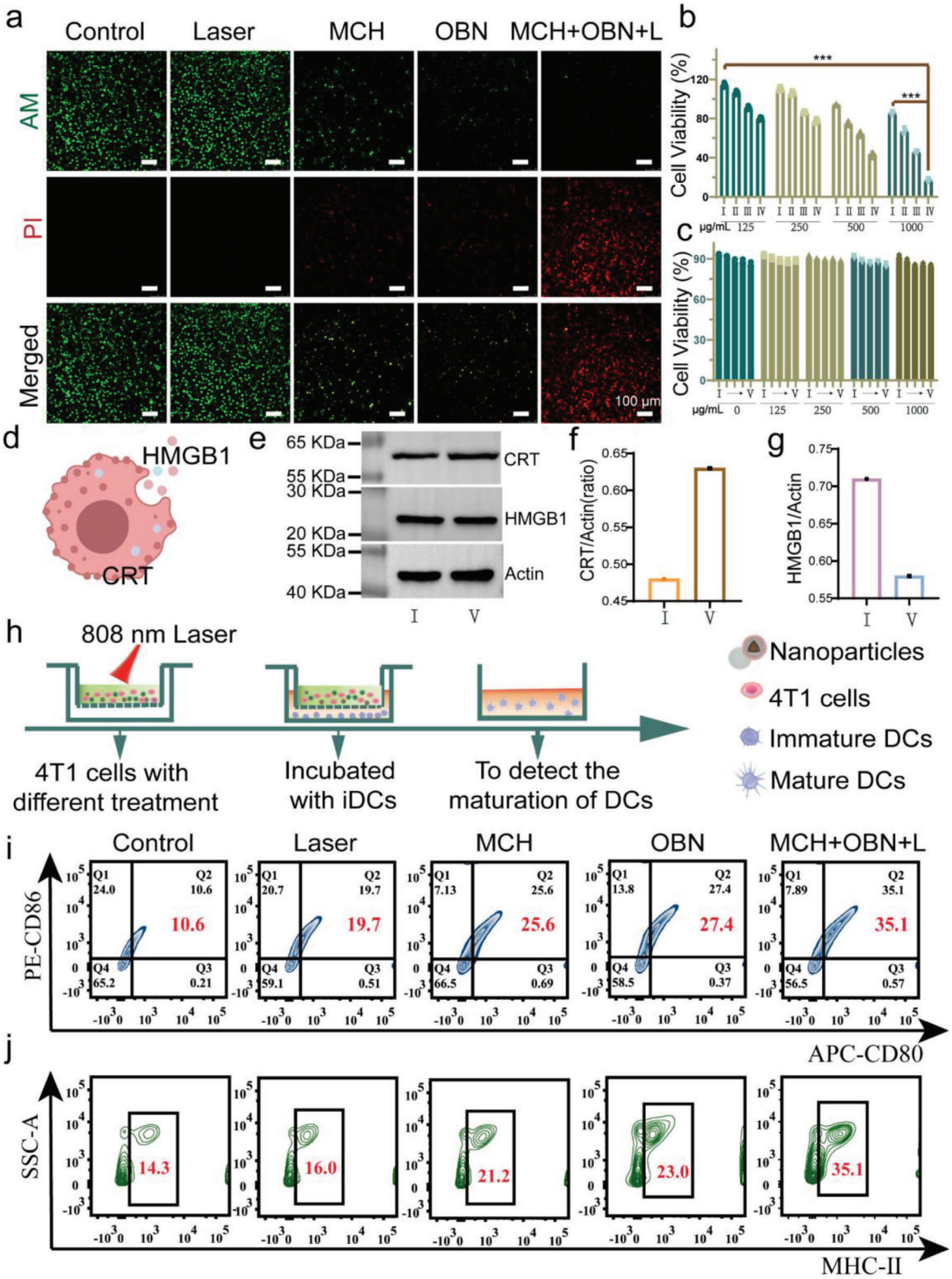


Figure 3. In vitro anti-tumor analysis and DCs mutation by MCH-OBN nanoplatform. a) CLSM of AM/PI staining (scale bar: 100 μm); b) Viabilities of 4T1 cells treated with I) MCH + OBN, II) MCH + Laser, III) OBN + Laser, and IV) MCH + OBN + Laser (125, 250, 500, and 1000 μg mL^{-1}) for 24 h (1 W cm^{-2}, 5 min); c) Viabilities of human umbilical vein endothelial cells (HUVEC) treated with I) MH, II) MCH, III) OB, IV) OBN, and V) MCH + OBN NPs (0, 125, 250, 500, and 1000 μg mL^{-1}) for 24 h; d–g) Western blotting and quantification of CRT and HMGB1; h) Schematic illustration of the transwell system: 4T1 cells with different treatments and DC2.4 cells were in the upper and lower part, respectively; i,j) Flow cytometry of CD80, CD86, and MHC-II. Data were presented as mean ± SD ($n = 3$), $^{**}p < 0.01$, $^{***}p < 0.001$.

© 2024 Wiley-VCH GmbH

16163028, 0, Downloaded from https://onlinelibrary.wiley.com/doi/10.1002/adfm.202315551 by Universidade Do Minho, Wiley Online Library on [26/03/2024]. See the Terms and Conditions (https://onlinelibrary.wiley.com/terms-and-conditions) on Wiley Online Library for rules of use; OA articles are governed by the applicable Creative Commons License

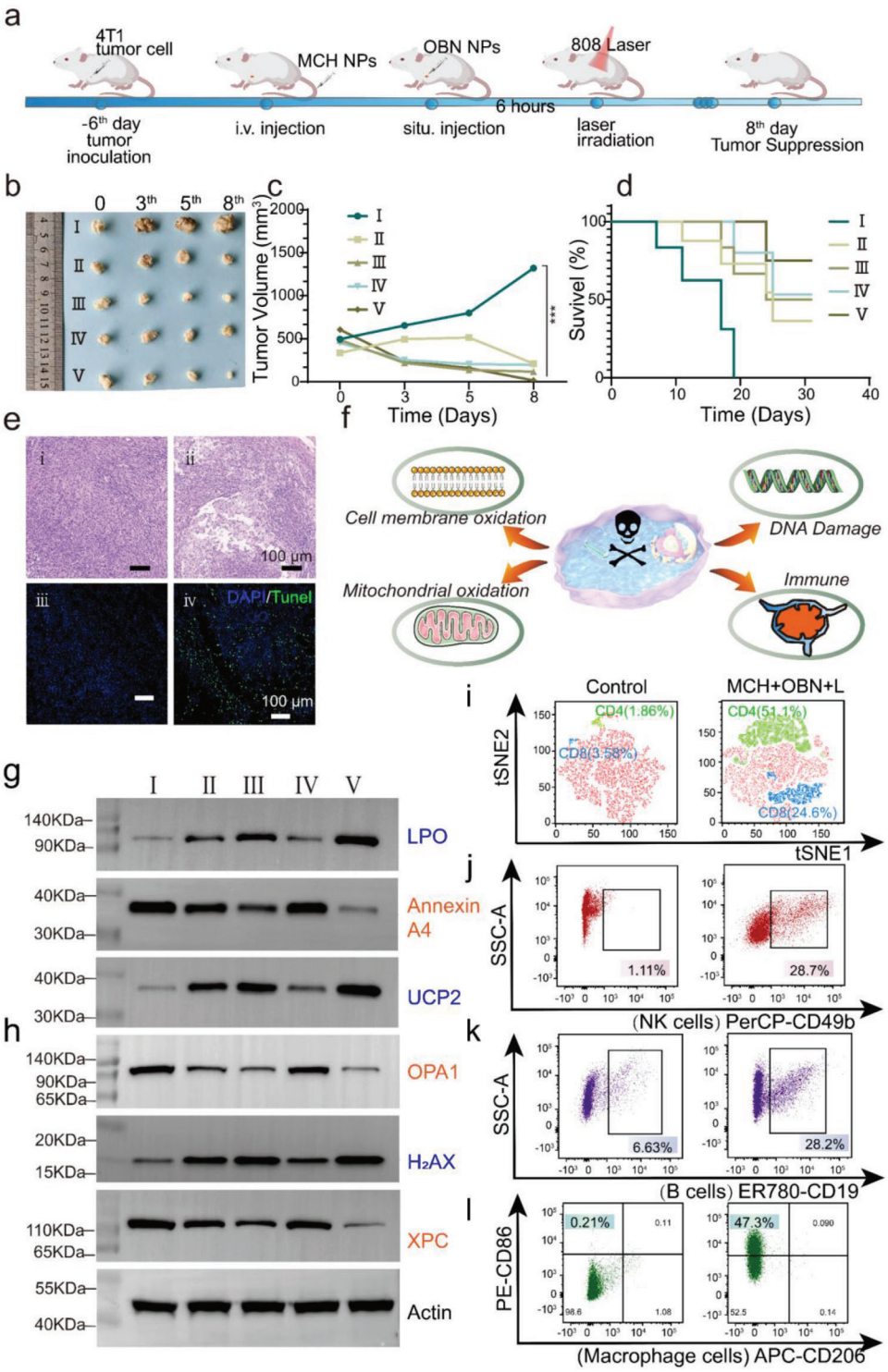


Figure 4. In vivo anti-tumor therapy and immune activation in wild-type Kunming mice. a) In vivo therapeutic scheme of MCH-OBN nanoplatform; b,c) Photographs and volume curves of the excised tumors from Kunming mice during 8 days; d) Survival curve of tumor-bearing mice; e) HE and Tunel staining of tumor tissue with different groups on the 8th day (i,iii: PBS, ii,iv: MCH + OBN + Laser); f) The presentation of tumor damage factors; g,h) Western blotting of LPO, AnnexinA4, UCP2, OPA1, H_2AX, and XPC of tumor tissues. Groups: I) Control, II) MH + Laser, III) MCH + Laser, IV) OBN + Laser, and V) MCH + OBN + Laser; i–l) Flow cytometric of T cells, B cells, NK cells, and M1 macrophage in lymph nodes of the control and MCH + OBN + Laser groups. Data were presented as mean± SD ($n = 3$), $^{**}p < 0.01$, $^{***}p < 0.001$.

© 2024 Wiley-VCH GmbH

16163028, 0, Downloaded from https://onlinelibrary.wiley.com/doi/10.1002/adfm.202315551 by Universidade Do Minho, Wiley Online Library on [26/03/2024]. See the Terms and Conditions (https://onlinelibrary.wiley.com/terms-and-conditions) on Wiley Online Library for rules of use; OA articles are governed by the applicable Creative Commons License

oxidation, and immunogenic death (Figure 4f). However, tumor cells could potentially initiate a damage recovery mechanism, thus leading to continued tumor reproduction. LPO and AnnexinA4 are commonly considered the markers of cell membrane oxidation and cell membrane oxidation repair,[53–55] respectively. UCP2 and OPA1 are the markers of mitochondrial damage and mitochondrial repair,[56,57] respectively. The content of H_2AX and XPC reflect the damage and repair of DNA, respectively.[58,59] As shown in Figure 4g,h, after MCH + OBN + Laser treatment, the upregulation of LPO, UCP2, and H_2AX and the downregulation of AnnexinA4, OPA1, and XPC suggested irreparable damage of tumor cells by impaired repair function of the cell membrane, DNA and mitochondria. Furthermore, after MCH-OBN + Laser treatment, the differentiation of CD4+/CD8+ T cells, B cells, NK cells, and M1 macrophage in the lymph nodes was significantly promoted (Figure 4i–l, and Figure S18, Supporting Information). Therefore, with the assistance of NO and RNS, the phototherapy strategy of the MCH-OBN nanoplatform achieved efficient death and irreversible damage of solid breast tumor cells, and also successfully reversed the "cold" immune state of tumor tissue into a "hot" immune state, which further accelerated tumor ablation.

2.5. In Vivo Anti-Tumor Therapy in Immunodeficient Mice

Through the above in vivo results, the significant activation of the immune system of wild-type Kunming mice during the anti-tumor phototherapy of MCH-OBN nanoplatform was demonstrated. To further investigate the role of immune activation during the anti-tumor phototherapy, the in vivo anti-tumor therapy of MCH-OBN nanoplatform for immunodeficient NOD-SCID mice was conducted (**Figure 5**a). For the first, the tumor temperature in vivo was measured in Figures S9 and S10, Supporting Information. After MCH NPs were injected via the tail vein of the normal mice and NOD mic, the accumulation of the nanoparticles at the tumor site was observed through photothermal imaging. Notably, the temperature at the tumor site of the normal mice increased to 52 °C at 6 h after administration, while under the same treatment condition, the temperature at the tumor site of the NOD mice was significantly lower than that of normal mice at 6 h after administration, suggesting that the heat conduction of MCH NPs was more significantly hindered in the immunodeficient environment. T cells, B cells, and NK cells showed almost complete absence in NOD-SCID mice and no obvious trend of activation after the same treatment of the MCH + OBN + Laser group, and macrophages were also maintained in M2-type (Figure 5b–e, and Figure S19, Supporting Information). These flow cytometry results demonstrated the maintenance of immune deficiency in NOD-SCID mice after phototherapy. Surprisingly, in the absence of immune systems, tumor tissue growth trends and the survival rate were almost consistent in the MCH + OBN + Laser and control groups (Figure 5f–h, and Figures S16 and S17, Supporting Information), indicating that anti-tumor phototherapy of MCH-OBN nanoplatform was almost completely ineffective for immunodeficient mice. Similarly, H&E staining (Figure 5i) and TUNEL assay (Figure 5j) showed only weak lesions in NOD-SCID tumors. In addition, the western-blotting results of LPO, UCP2, H_2AX, AnnexinA4, OPA1, and XPC in NOD-SCID mice were completely opposite to that of wild-type mice during the treatment of MCH-OBN nanoplatform (Figure 5k,l), verifying ineffective phototherapy in immunodeficient mice. Therefore, these anti-tumor effect comparisons between wild-type mice and immunodeficient mice demonstrated the close reliance on the anti-tumor effect of phototherapy on immune activation, suggesting that the immune system may not only directly kill tumor cells, but also participate in other pathways to determine the effectiveness of anti-tumor phototherapy strategy.

2.6. Expression Comparison of CAF-Related Factors in Wild-Type and NOD-SCID Mice

To analyze the specific mechanisms by which the immune system regulated the effect of phototherapy on tumor cell killing, tumor tissues of wild-type mice and immunodeficient NOD-SCID mice treated with MCH-OBN nanoplatform were conducted for further analysis. Since both thermal ablation and ROS face the issues of spatial conduction and quenching when killing tumor cells, the differences in exoprotein expression around the two types of mouse tumor cells are the focus of the investigation. Fibronectin (FN), α-smooth muscle actin (α-SMA), and collagen, which are the markers of CAFs,[60] showed significant upregulation in tumor tissues of NOD-SCID mice compared with those of wild-type mice (**Figure 6**a,b). It was fully demonstrated that the activated immune system showed significant inhibition of the proliferation of tumor-associated fibroblasts (CAFs) in tumor tissues, suggesting that the anti-tumor failure of the MCH-OBN nanoplatform in NOD-SCID mice may be related to the presence of heavily distributed CAF in tumor tissues with "cold" immune status. After treatment with the MCH-OBN nano platform, the expression of ICD-related proteins CRT and HMGB1 did not change in NOD-SCID mouse tumors but was significantly upregulated in wild-type mouse tumors (Figure 6c,d). Meanwhile, MCH-OBN phototherapy significantly improved the upregulation of immune killer factors such as granzyme B (GZMB), interleukin 2 (IL-2), and tumor necrosis faction-α (TNF-α) in wild-type tumors, but had no similar effect on NOD-SCID tumors (Figure 6e,f). Current studies have confirmed that CAFs promote extracellular matrix curing by secreting a large amount of collagen, fibronectin, and other factors, inhibit immune cells recruited by tumor chemokines, and resist the penetration of anti-tumor drugs.[61] Therefore, it was speculated that the differences between tumor therapeutic efficacy and physiological indexes of wild-type mice and NOD-SCID mice induced by phototherapy of MCH-OBN nanoplatforms are significantly related to the differentially expressed CAFs and their physical barriers under different immune status.

2.7. In Vitro Analysis of CAFs Regulating the Anti-Tumor Mechanism of Phototherapy

To confirm the decisive role of CAFs in regulating the anti-tumor effect of phototherapy, CD45-/CD31-/FAP+ tumor-associated fibroblasts (CAFs) were separated from tumor single-cell suspension of 4T1-bearing mice by flow cytometry. Then, separated CAFs were co-cultured with 4T1 cells to evaluate the effect of

© 2024 Wiley-VCH GmbH

16163028, 0, Downloaded from https://onlinelibrary.wiley.com/doi/10.1002/adfm.202315551 by Universidade Do Minho, Wiley Online Library on [26/03/2024]. See the Terms and Conditions (https://onlinelibrary.wiley.com/terms-and-conditions) on Wiley Online Library for rules of use; OA articles are governed by the applicable Creative Commons License

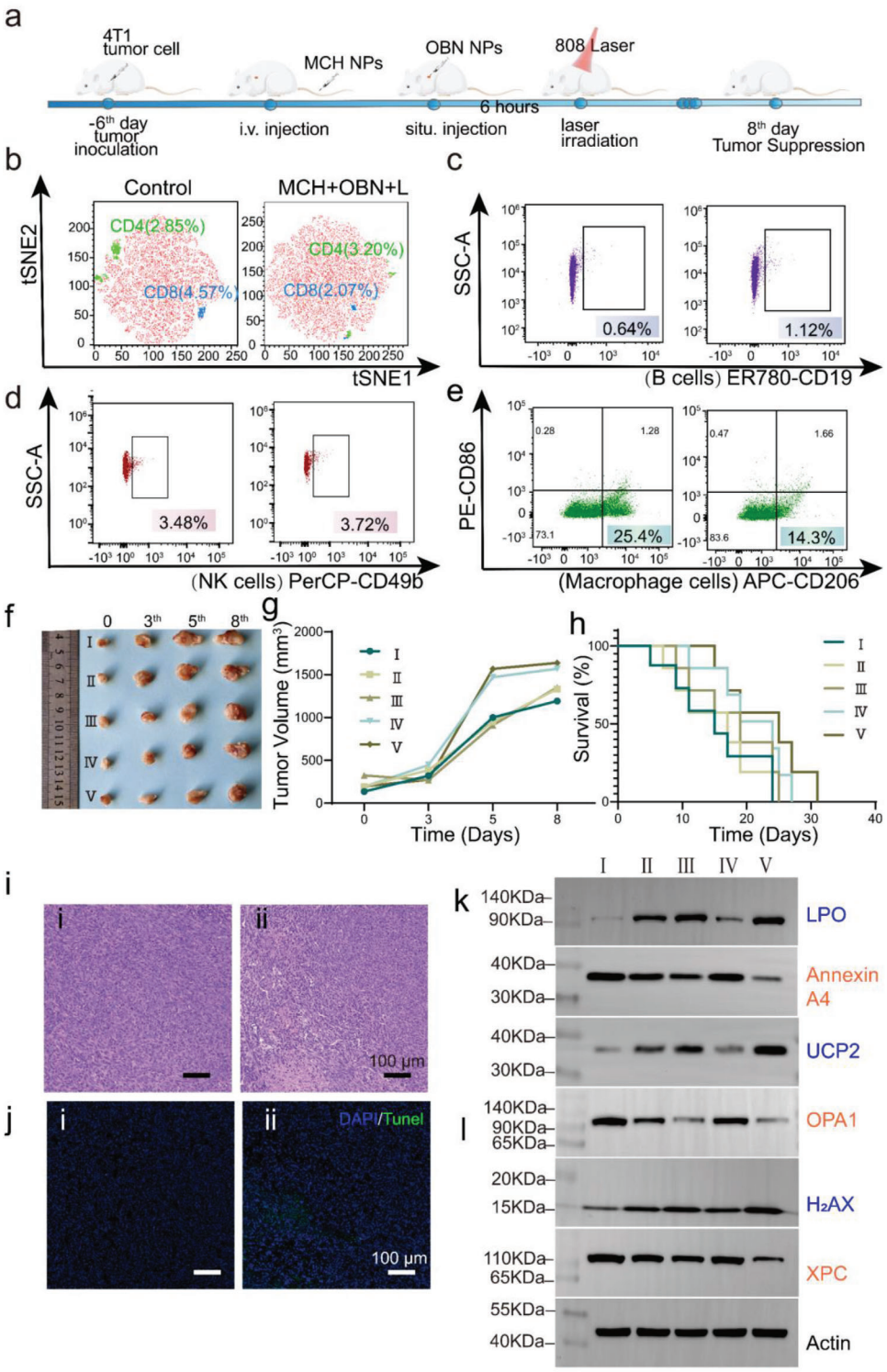


Figure 5. In vivo anti-tumor therapy in NOD-SCID mice. a) Therapeutic scheme of MCH-OBN nanoplatform in vivo; b–e) Flow cytometry of T cells, B cells, NK cells, and phenotype of macrophages in lymph nodes of NOD-SCID tumor-bearing mice; f,g) Photographs and volume curves of tumors from NOD-SCID mice; h) Survival curve of tumor-bearing NOD-SCID mice; i,j) HE staining and TUNEL staining of tumor tissues in the NOD-SCID mice on the 8th day (i: PBS, ii: MCH + OBN + Laser); k,l) Western blotting of LPO, AnnexinA4, UCP2, OPA1, H_2AX, and XPC of tumor tissues in NOD-SCID mice. Groups: I) Control, II) MH + Laser, III) MCH + Laser, IV) OBN + Laser, V) MCH + OBN + Laser. Data were presented as mean ± SD ($n = 3$), $^{**}p < 0.01$, $^{***}p < 0.001$.

© 2024 Wiley-VCH GmbH

16163028, 0, Downloaded from https://onlinelibrary.wiley.com/doi/10.1002/adfm.202315551 by Universidade Do Minho, Wiley Online Library on [26/03/2024]. See the Terms and Conditions (https://onlinelibrary.wiley.com/terms-and-conditions) on Wiley Online Library for rules of use; OA articles are governed by the applicable Creative Commons License

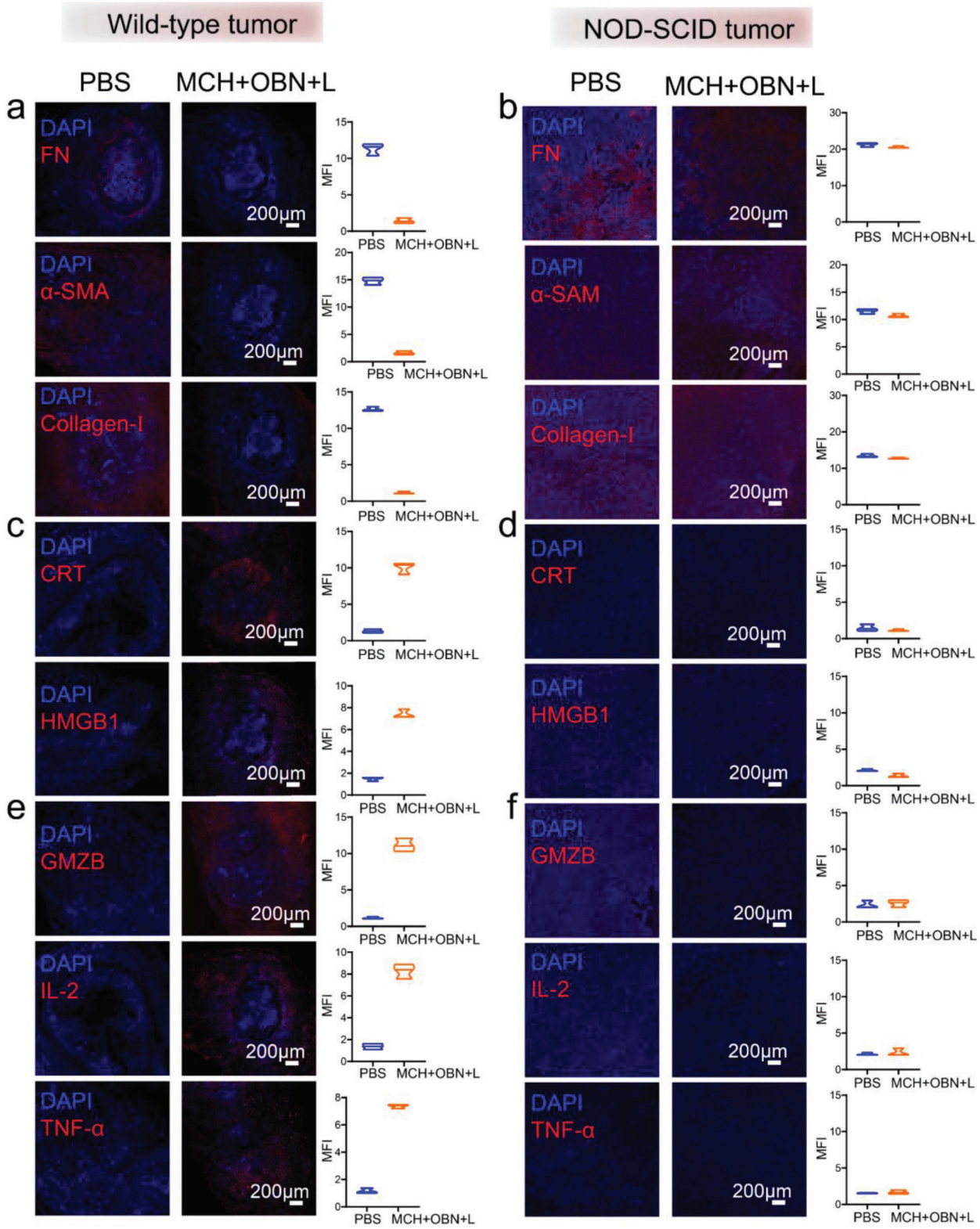


Figure 6. Expression comparison of CAFs-related factors in wild-type and NOD-SCID mice. a,b) Immunohistochemical analysis of FN, α-SMA, and collagen-I in wild-type mice and NOD-SCID mice; c,d) Immunohistochemical analysis of CRT and HMGB1 in wild-type mice and NOD-SCID mice; e,f) Immunohistochemical analysis of GZMB, IL-2, and TNF-α in wild-type mice and NOD-SCID mice. Scale bar: 200 μm.

© 2024 Wiley-VCH GmbH

16163028, 0, Downloaded from https://onlinelibrary.wiley.com/doi/10.1002/adfm.202315551 by Universidade Do Minho, Wiley Online Library on [26/03/2024]. See the Terms and Conditions (https://onlinelibrary.wiley.com/terms-and-conditions) on Wiley Online Library for rules of use; OA articles are governed by the applicable Creative Commons License

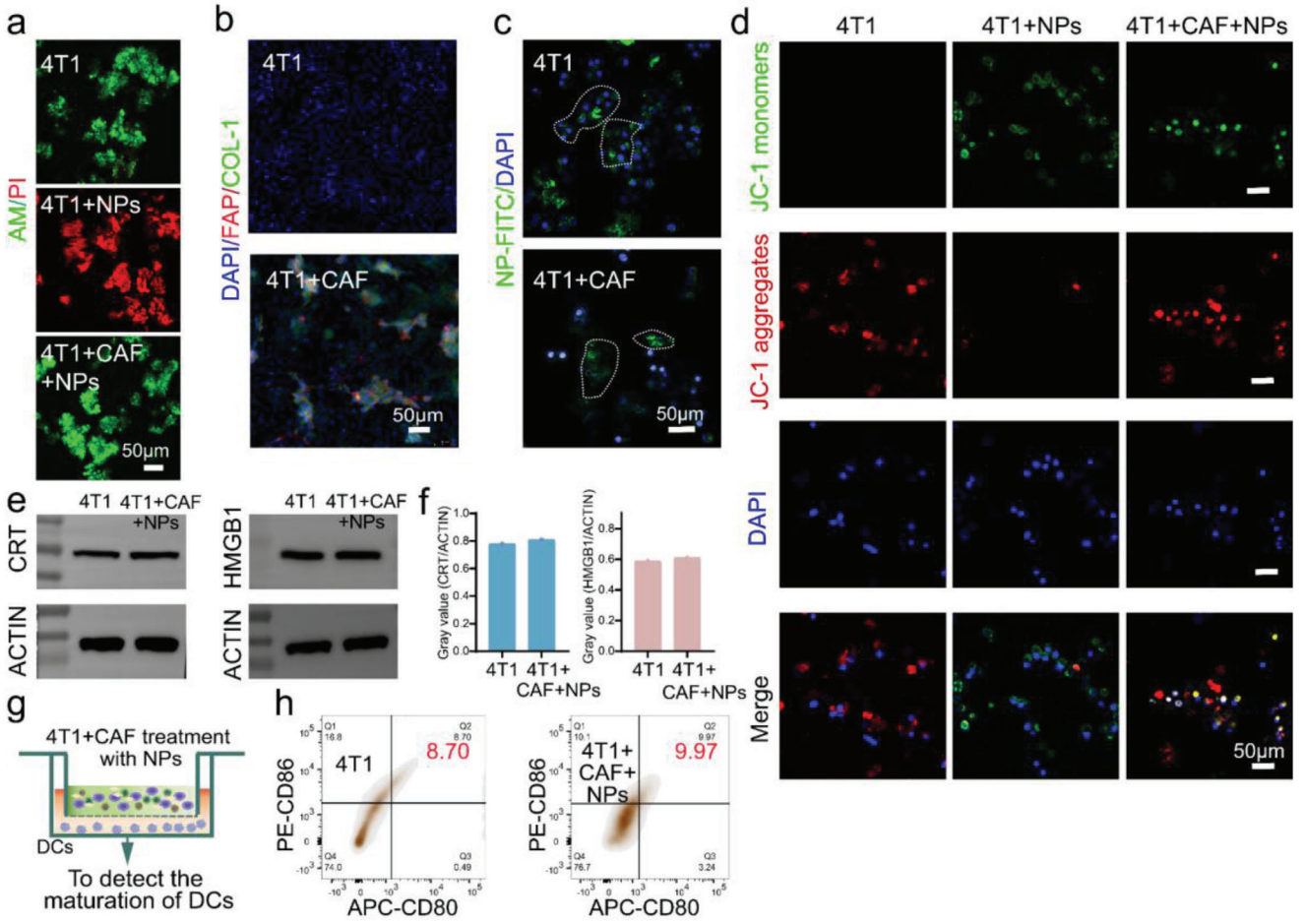


Figure 7. In vitro analysis of CAFs regulating the anti-tumor mechanism of phototherapy. a) CLSM images of AM/PI staining for 4T1, 4T1+NPs, and 4T1+CAF+NPs groups (scale bar: 100 μm); b) CLSM images of CAF cells (FAP+) co-located with collagen-I (blue was for DAPI fluorescence imaging of the nucleus; green was for FITC fluorescence imaging of collagen-I; red was for fluorescence imaging of CAFs); c) The uptake of FITC-labeled NPs by 4T1 cells with or without CAFs; d) Mitochondrial membrane potential of 4T1, 4T1+CAF, and 4T1+CAF+NPs groups (scale bar: 50 μm); e,f) Western-blotting and quantification of CRT and HMGB1 of 4T1 and 4T1+CAF+NPs groups; g) Schematic illustration of the transwell system. The CAF+NPs treated 4T1 cells were in the upper part and the DC2.4 cells were in the lower part. h) Flow cytometry of DCs (CD80+/CD86+).

CAFs on 4T1 cells in response to MCH-OBN nanoplatform treatment. Compared with 4T1 cells cultured alone, apoptosis of CAFs co-cultured 4T1 cells was significantly reduced when treated by MCH-OBN phototherapy (**Figure** 7a), demonstrating the participation of CAFs in the protection of 4T1 cells from phototherapy. In order to further explore the mechanism of CAFs helping tumor cells resist phototherapy killing, collagen secretion, and nanoparticle phagocytosis in 4T1 tumor microenvironment under CAFs co-culture were investigated. Co-localization of CAFs (FAP+) and collagen-I (Figure 7b) proved the secretion of collagen by CAFs as well as the existence of a collagen barrier supporting provided by CAFs for 4T1 cells, thus effectively inhibiting the heat conduction and the spatial transmission of ROS and RNS during phototherapy. Moreover, As indicated by the inner region of the dashed line in Figure 7c, when CAFs were co-cultured with 4T1 cells, the nanoparticles and cells (neither 4T1 cells nor CAFs) failed to colocalize, while a large number of nanoparticles were localized inside the tumor cells when only 4T1 cells were present (blue was for DAPI fluorescence imaging of the nucleus, and green was for FITC fluorescence imaging of MCH NPs). This suggested that the massive secretion of extracellular collagen most likely severely hinders the endocytosis behavior of nanoparticles. Therefore, CAFs and the collagen secreted by them can act as a "protective barrier" in the 3D tumor tissue, which will become a huge obstacle for reactive oxygen species and heat conduction which are extremely sensitive to distance. Moreover, compared with the significant decrease of mitochondrial membrane potential in 4T1 cells cultured alone, the mitochondrial membrane potential of CAFs co-cultured 4T1 cells showed almost no change after MCH-OBN treatment (Figure 7d). More surprisingly, the expressions of CRT and HMGB1 in CAFs co-cultured 4T1 cells were not activated after MCH-OBN treatment (Figure 7e,f), thus failing to promote the maturation of DC cells (Figure 7g,h). By combining the results of Figure 5 with those of Figure 7, it was concluded that the presence of CAFs has a significant impact on the anti-tumor effect of phototherapy. When phototherapy was applied to wild-type tumor-bearing mice, it could effectively activate the immune system in

© 2024 Wiley-VCH GmbH

16163028, 0, Downloaded from https://onlinelibrary.wiley.com/doi/10.1002/adfm.202315551 by Universidade Do Minho, Wiley Online Library on [26/03/2024]. See the Terms and Conditions (https://onlinelibrary.wiley.com/terms-and-conditions) on Wiley Online Library for rules of use; OA articles are governed by the applicable Creative Commons License

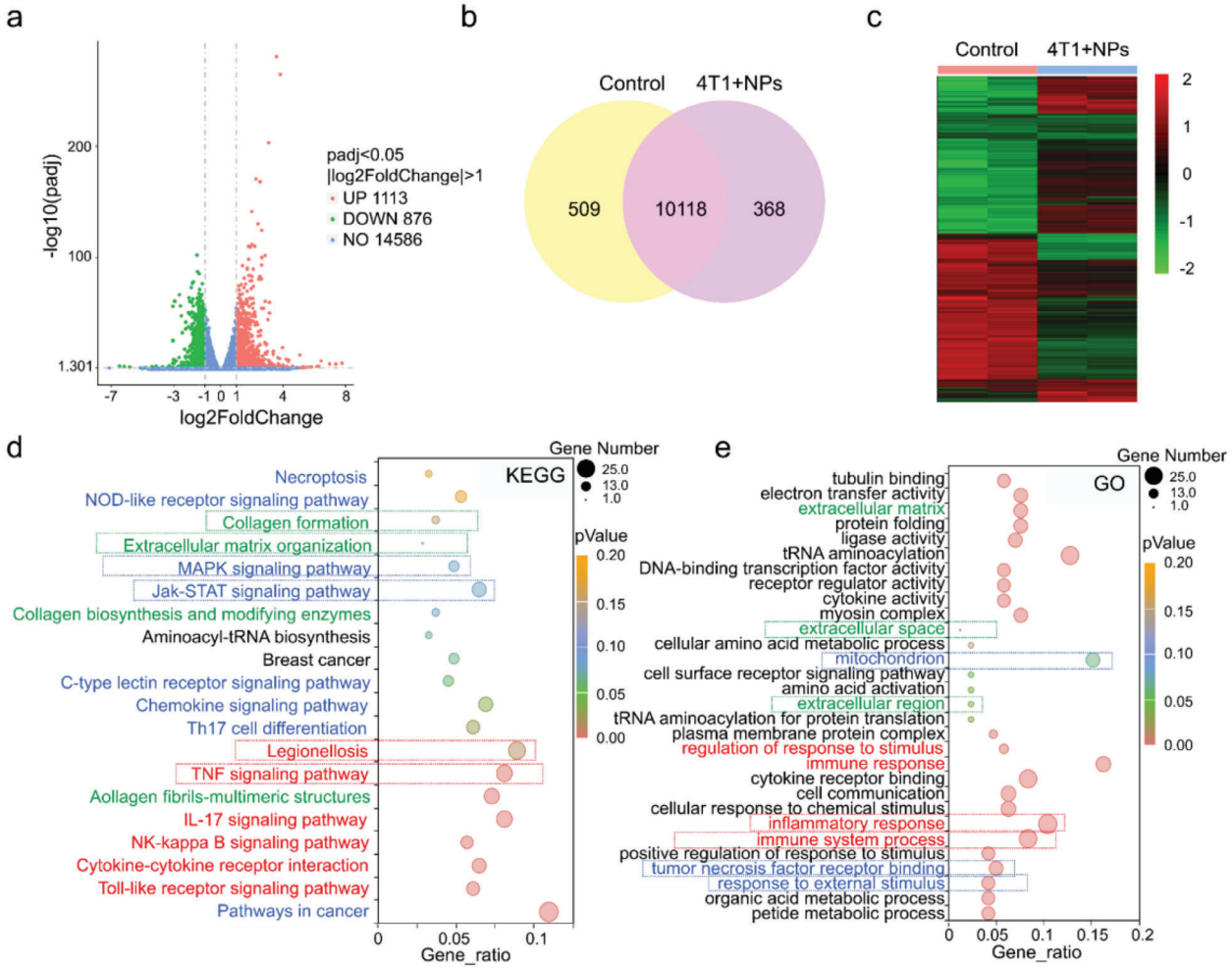


Figure 8. Transcriptional analysis of 4T1 tumor cells after the MCH-OBN + Laser treatment. a–c) Volcano plot, Venn diagram, and heatmap showing differentially expressed genes with significance; d) The bubble maps showing the significant enrichment of immune(red)/ apoptosis(blue)/extracellular matrix(green)-related pathways by KEGG enrichment analysis. e) The bubble maps show the significant enrichment of immune(red)/ apoptosis(blue)/extracellular matrix(green)-related pathways by GO enrichment analysis.

vivo and promote the tumor site to enter an immune "hot" state. The activated immune system in turn enhanced the anti-tumor efficacy of phototherapy by inhibiting the proliferation of CAFs and destroying the extracellular barrier. However, when phototherapy was applied to immunodeficient tumor-bearing mice, the absence of immune cells resulted in excessive CAF proliferation and extracellular barrier stabilization, and this enhanced immune "cold" state further isolated the penetration and cell killing of phototherapy vectors in tumor tissues. Therefore, CAFs effectively blocked heat conduction and ROS/RNS transmission during phototherapy by constructing a cell/protein barrier, thus significantly reversing MCH-OBN nanoplatform's attack on 4T1 cells and immune activation.

2.8. Transcriptional Analysis

To further confirm the protection of 4T1 cells by CAFs during phototherapy, the transcriptional results of 4T1 cells cultured alone and 4T1 cells co-cultured with CAFs after the same MCH-OBN nanoplatform treatment were analyzed. Compared with untreated 4T1 cells, the expression of 1989 genes was significantly affected in 4T1 cells treated with MCH-OBN nanoplatform, of which 1113 genes were upregulated, and 876 genes were significantly downregulated ($p < 0.05$, log2FoldChange| > 1) (**Figure** 8a–c). Through Gene Ontology (GO) and the Kyoto Encyclopedia of Genes and Genomes (KEGG), these differentially expressed genes were found to be associated with multiple apoptosis and immune activation signaling pathways. KEGG analysis demonstrated that MCH-OBN nanoplatform treatment promoted the activation of pathways related to immune activation (red) in the tumor microenvironment (including cytokine-cytokine receptor interaction, IL-17 signaling pathway, toll-like receptor signaling pathway, and TNF signaling pathway), as well as apoptosis-related pathways (including Jak-STAT signaling pathway and MAPK signaling pathway) (Figure 8d). GO enrichment analysis showed that after MCH-OBN nano platform treatment, immune

© 2024 Wiley-VCH GmbH

16163028, 0, Downloaded from https://onlinelibrary.wiley.com/doi/10.1002/adfm.202315551 by Universidade Do Minho, Wiley Online Library on [26/03/2024]. See the Terms and Conditions (https://onlinelibrary.wiley.com/terms-and-conditions) on Wiley Online Library for rules of use; OA articles are governed by the applicable Creative Commons License

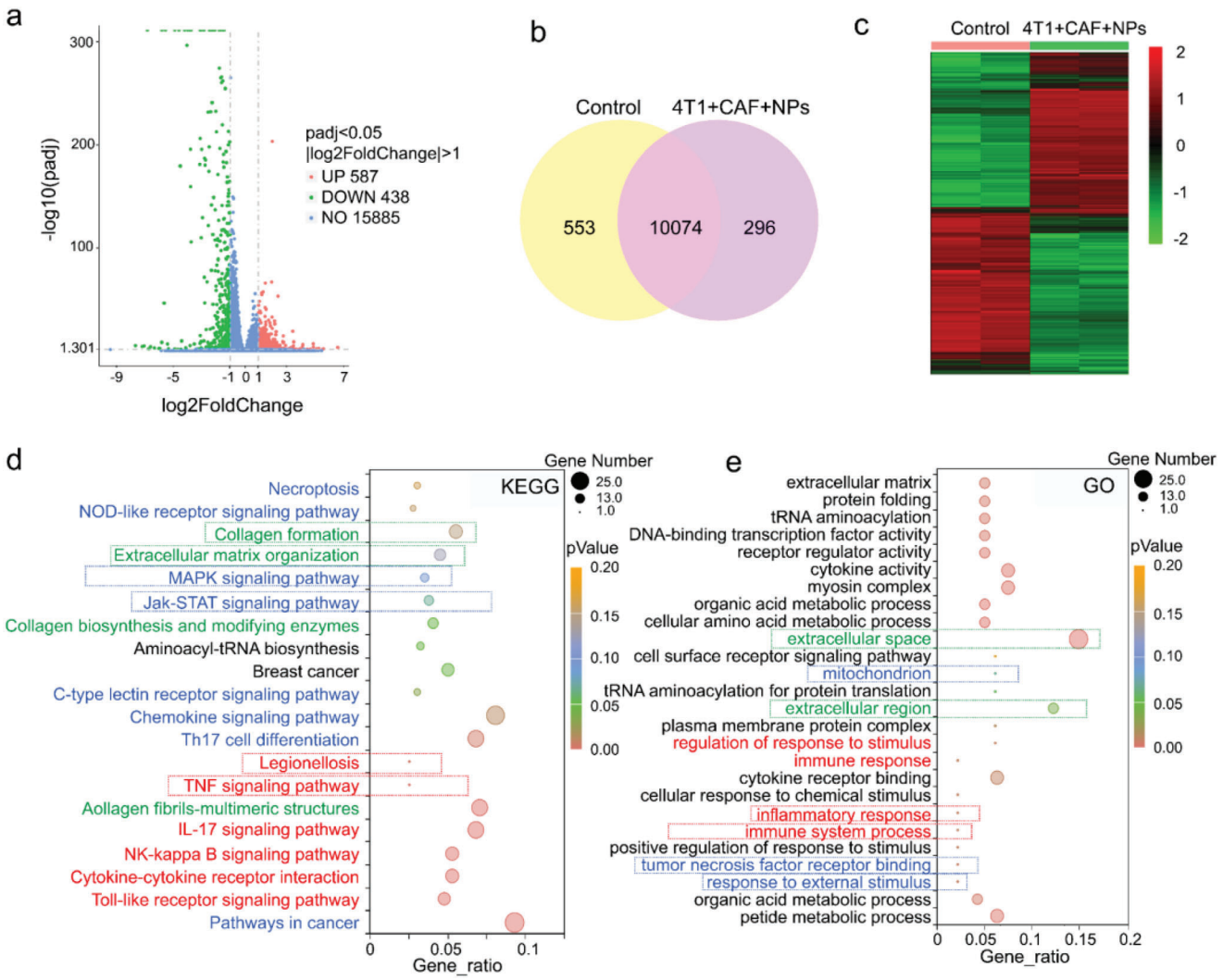


Figure 9. Transcriptional analysis of the 4T1 tumor cells cultured with CAF after the MCH-OBN + Laser treatment. a–c) Volcano plot, Venn diagram, and heatmap showing differentially expressed genes with significance; d) The bubble maps showing the significant enrichment of immune (red)/apoptosis (blue)/extracellular matrix (green)-related pathways by KEGG enrichment analysis. e) The bubble maps show the significant enrichment of immune (red)/apoptosis (blue)/extracellular matrix (green)-related pathways by GO enrichment analysis.

system process, immune response, and cytokine receptor binding in 4T1 cells, as well as TNF receptor binding and extracellular region signaling pathways were significantly upregulated (Figure 8e). The above-upregulated signaling pathways are located upstream of the immunomodulatory process, which implies an enhanced systemic immune response after treatment of the MCH-OBN nanoplatform.

In addition, transcriptome analysis of 4T1 cells co-cultured with CAFs showed that only 587 genes were upregulated and 483 genes were downregulated after treatment of MCH-OBN nanoplatform ($p < 0.05$, log2FoldChange| > 1) (**Figure** 9a–c). KEGG analysis of differential genes showed that the upregulated regulatory signaling pathways in CAFs-cocultured 4T1 cells were significantly correlated with the expression of extracellular matrix such as collagen formation and extracellular matrix organization (green markers). This suggests that CAFs not only secreted large amounts of ECM themselves but also induced ECM secretion from tumor cells, thus establishing a dense ECM environment that resists drug penetration. KEGG analysis also confirmed that the involvement of CAFs could inhibit the tumor immune activation pathways including legionellosis and TNF signaling pathways (red marks), as well as tumor apoptosis pathway including Jak-STAT signaling pathway and MAPK signaling pathway (blue) (Figure 9d). Similarly, GO analysis also confirmed the activation of extracellular matrix secretion signaling pathways by CAFs, including extracellular space and extracellular region. The promotion of immune activation (red markers) and the inhibition of tumor apoptosis (marked in blue) by CAFs was also confirmed in Figure 9e. Therefore, the above results provide evidence that CAFs promote the secretion of tumor extracellular matrix and inhibit the immune microenvironment of the tumor. Therefore, the differences in the cellular and genetic behaviors of 4T1 cells and 4T1 cells co-cultured with CAFs in response to phototherapy suggested that the abundance of CAFs in immune "cold" tumor

© 2024 Wiley-VCH GmbH

16163028, 0, Downloaded from https://onlinelibrary.wiley.com/doi/10.1002/adfm.202315551 by Universidade Do Minho, Wiley Online Library on [26/03/2024]. See the Terms and Conditions (https://onlinelibrary.wiley.com/terms-and-conditions) on Wiley Online Library for rules of use; OA articles are governed by the applicable Creative Commons License

tissues not only hinders the heat conduction and the attack of active small molecules on tumor cells during phototherapy but also significantly inhibits the subsequent immune activation. On the contrary, in the immune "hot" tumor tissue, the highly activated immune members inhibit the proliferation of CAFs and break the protection given by CAFs to tumor cells, which in turn promotes the thermal ablation and killing of tumor cells by active small molecules during phototherapy.

3. Conclusion

Inspired by the knowledge that the anti-tumor effect of chemotherapy drugs depended on the activity of the immune system, this work was the first to focus on the effect of immune activation status on the anti-tumor efficacy of phototherapy. First, the MCH-OBN nanoplatform provided the NO/RNS-assisted phototherapy on tumors under the premise of low toxicity and the simplified preparation process, demonstrating a promising tumor-killing effect and significant immune activation. Moreover, the difference in tumor efficacy of the MCH-OBN nanoplatform on wild-type and immunodeficient mice confirmed the strong dependence of phototherapy on immune activation status. Importantly, this study confirmed that the immune system promoted the killing of tumor cells in phototherapy by destroying the physical barrier of CAFs to tumor cells, thus providing the anti-tumor effectiveness of phototherapy. This work defines the regulation mechanism of immune activation during phototherapy, which is of great significance for the clinical development of CAFs-targeting anti-tumor strategies of immune-assisted phototherapy.

Supporting Information

Supporting Information is available from the Wiley Online Library or from the author.

Acknowledgements

M.D. and H.C. contributed to the work equally and should be regarded as co-first authors. This work was supported by the National Natural Science Foundation of China (Grant No. 32101137), Natural Science Foundation of Shandong Province (Grant No. ZR2022MH187), National Key Research and Development Project of China (Grant No. 2023YFFO715101), Young Taishan Scholars Program of Shandong Province (Grant No. tsqn202306272), Innovation and technology program for the excellent youth scholars of higher education of Shandong province (Grant No. 2019KJE015), Traditional Chinese Medicine Science and Technology Project of Shandong province (Grant No. 2021Q069), the Leading Project of Science and Technology of Yantai Development Zone (Grant No. 2021RC016), and Open Projects Fund of Shandong Key Laboratory of Carbohydrate Chemistry and Glycobiology, Shandong University (Grant No. 2023CCG11).

Conflict of Interest

The authors declare no conflict of interest.

Author Contributions

M.D.: Conceptualization, methodology, data curation, writing – original draft; H.C.: Data curation, validation; C.F.G.: Resources, writing – review & editing; R.L.R.: Resources, writing – review & editing; L.W.: Resources; F.Z.: Investigation. Y.L.: Investigation; T.W.: Investigation; Q.Z.: Validation, funding acquisition; J.S.: Conceptualization, funding acquisition. X.K.: Conceptualization, supervision, funding acquisition.

Data Availability Statement

Research data are not shared.

Keywords

anti-tumor mechanisms, cancer-associated fibroblasts, immune activation, phototherapy

Received: December 6, 2023
Revised: January 16, 2024
Published online:

[1] A. Costa, Y. Kieffer, A. Scholer-Dahirel, F. Pelon, B. Bourachot, M. Cardon, P. Sirven, I. Magagna, L. Fuhrmann, C. Bernard, C. Bonneau, M. Kondratova, I. Kuperstein, A. Zinovyev, A. M. Givel, M. C. Parrini, V. Soumelis, A. Vincent-Salomon, F. Mechta-Grigoriou, *Cancer Cell* **2018**, *33*, 463.
[2] E. A. De Jaeghere, H. G. Denys, O. De Wever, *Trends Cancer* **2019**, *5*, 704.
[3] P. Comoli, C. Chabannon, U. Koehl, F. Lanza, A. Urbano-Ispizua, M. Hudecek, A. Ruggeri, S. Secondino, C. Bonini, P. Pedrazzoli, *Ann. Oncol.* **2019**, *30*, 1740.
[4] N. Liu, R. Zhang, Q. Shi, H. Jiang, Q. Zhou, *Bioorg. Chem.* **2023**, *136*, 106550.
[5] S. Li, W. Zhang, R. Xing, C. Yuan, H. Xue, X. Yan, *Adv. Mater.* **2021**, *33*, 2100595.
[6] C. Wang, P. Li, L. Liu, H. Pan, H. Li, L. Cai, Y. Ma, *Biomaterials* **2016**, *79*, 88.
[7] Q. Feng, Y. Li, N. Wang, Y. Hao, J. Chang, Z. Wang, X. Zhang, Z. Zhang, L. Wang, *Small* **2020**, *16*, 2002138.
[8] W. Li, J. Yang, L. Luo, M. Jiang, B. Qin, H. Yin, C. Zhu, X. Yuan, J. Zhang, Z. Luo, Y. Du, Q. Li, Y. Lou, Y. Qiu, J. You, *Nat. Commun.* **2019**, *10*, 3349.
[9] L. Huang, Y. Li, Y. Du, Y. Zhang, X. Wang, Y. Ding, X. Yang, F. Meng, J. Tu, L. Luo, C. Sun, *Nat. Commun.* **2019**, *10*, 4871.
[10] J. Huang, X. Leng, T. Jiang, L. Xu, J. Zheng, M. Fang, J. Wang, Z. Wang, L. Zhang, *Mater. Today Bio* **2023**, *19*, 100555.
[11] K. Ni, T. Luo, G. Lan, A. Culbert, Y. Song, T. Wu, X. Jiang, W. Lin, *Angew. Chem.* **2020**, *59*, 1108.
[12] X. Duan, C. Chan, W. Lin, *Angew. Chem.* **2019**, *58*, 670.
[13] Z. Fan, H. Liu, Y. Xue, J. Lin, Y. Fu, Z. Xia, D. Pan, J. Zhang, K. Qiao, Z. Zhang, Y. Liao, *Bioact. Mater.* **2021**, *6*, 312.
[14] W. Song, P. Jia, T. Zhang, K. Dou, L. Liu, Y. Ren, F. Liu, J. Xue, M. S. Hasanin, H. Qi, Q. Zhou, *J. Nanobiotechnol.* **2022**, *20*, 289.
[15] Q. Chen, C. Liu, C. Liu, D. Zhong, S. Hua, J. He, K. Wang, M. Zhou, *Nano Today* **2021**, *41*, 101311.
[16] Y. Chen, Y. Huang, Q. Li, Z. Luo, Z. Zhang, H. Huang, J. Sun, L. Zhang, R. Sun, D. J. Bain, J. F. Conway, B. Lu, S. Li, *Nat. Nanotechnol.* **2023**, *18*, 193.
[17] Z. Zhang, Y. X. Yue, Q. Li, Y. Wang, X. Wu, X. Li, H. B. Li, L. Shi, D. S. Guo, Y. Liu, *Adv. Funct. Mater.* **2023**, *33*, 2213967.
[18] E. Koncina, M. Nurmik, V. I. Pozdeev, C. Gilson, M. Tsenkova, R. Begaj, S. Stang, A. Gaigneaux, C. Weindorfer, F. Rodriguez, M. Schmoetten, E. Klein, J. Karta, V. S. Atanasova, K. Grzyb, P. Ullmann, R. Halder, M. Hengstschlager, J. Graas, V. Augendre, Y. E. Karapetyan,

© 2024 Wiley-VCH GmbH

16163028, 0, Downloaded from https://onlinelibrary.wiley.com/doi/10.1002/adfm.202315551 by Universidade Do Minho, Wiley Online Library on [26/03/2024]. See the Terms and Conditions (https://onlinelibrary.wiley.com/terms-and-conditions) on Wiley Online Library for rules of use; OA articles are governed by the applicable Creative Commons License

L. Kerger, N. Zuegel, A. Skupin, S. Haan, J. Meiser, H. Dolznig, E. Letellier, *Nat. Commun.* **2023**, *14*, 4251.
[19] D. Hu, Z. Li, B. Zheng, X. Lin, Y. Pan, P. Gong, W. Zhuo, Y. Hu, C. Chen, L. Chen, J. Zhou, L. Wang, *Cancer Commun.* **2022**, *42*, 401.
[20] M. Michaud, I. Martins, A. Q. Sukkurwala, S. Adjemian, Y. Ma, P. Pellegatti, S. Shen, O. Kepp, M. Scoazec, G. Mignot, S. Rello-Varona, M. Tailler, L. Menger, E. Vacchelli, L. Galluzzi, F. Ghiringhelli, F. di Virgilio, L. Zitvogel, G. Kroemer, *Science* **2011**, *334*, 1573.
[21] A. Chakravarthy, L. Khan, N. P. Bensler, P. Bose, D. D. De Carvalho, *Nat. Commun.* **2018**, *9*, 4692.
[22] J. Liu, Y. Wang, C. Mu, M. Li, K. Li, S. Li, W. Wu, L. Du, X. Zhang, C. Li, W. Peng, J. Shen, Y. Liu, D. Yang, K. Zhang, Q. Ning, X. Fu, Y. Zeng, Y. Ni, Z. Zhou, Y. Liu, Y. Hu, X. Zheng, T. Wen, Z. Li, Y. Liu, *Nat. Commun.* **2022**, *13*, 4308.
[23] P. D Carvalho, C. F. Guimarães, A. P. Cardoso, S. Mendonça, Â. M. Costa, M. J. Oliveira, S. Velho, *Cancer Res.* **2018**, *78*, 7.
[24] H. Yoon, C. M. Tang, S. Banerjee, A. L. Delgado, M. Yebra, J. Davis, J. K. Sicklick, *Oncogenesis* **2021**, *10*, 13.
[25] Y. Yan, X. Chen, X. Wang, Z. Zhao, W. Hu, S. Zeng, J. Wei, X. Yang, L. Qian, S. Zhou, L. Sun, Z. Gong, Z. Xu, *J. Exp. Clin. Cancer Res.* **2019**, *38*, 171.
[26] X. Li, T. Yong, Z. Wei, N. Bie, X. Zhang, G. Zhan, J. Li, J. Qin, J. Yu, B. Zhang, L. Gan, X. Yang, *Nat. Commun.* **2022**, *13*, 2794.
[27] C. F. Guimarães, L. Gasperini, A. P. Marques, R. L. Reis, *Nat. Rev. Mater.* **2020**, *5*, 351.
[28] C. F. Guimarães, L. Gasperini, A. P. Marques, R. L. Reis, *Appl. Mater. Today* **2021**, *23*, 101013.
[29] H. Shin, Y. Kim, S. Jon, *ACS Nano* **2023**, *17*, 10337.
[30] Z. Yuan, Y. Li, S. Zhang, X. Wang, H. Dou, X. Yu, Z. Zhang, S. Yang, M. Xiao, *Mol. Cancer* **2023**, *22*, 48.
[31] X. He, X. Chen, L. Liu, Y. Zhang, Y. Lu, Y. Zhang, Q. Chen, C. Ruan, Q. Guo, C. Li, T. Sun, C. Jiang, *Adv. Sci.* **2018**, *5*, 1701070.
[32] E. Noguera-Ortega, L. Todd, J. Monslow, J. Sun, S. M. Albelda, E. Pure, *Cancer Immunol. Res.* **2020**, *8*, A62.
[33] Y. C. Sung, P. R. Jin, L. A. Chu, F. F. Hsu, M. R. Wang, C. C. Chang, S. J. Chiou, J. T. Qiu, D. Y. Gao, C. C. Lin, Y. S. Chen, Y. C. Hsu, J. Wang, F. N. Wang, P. L. Yu, A. S. Chiang, A. Y. Wu, J. J. Ko, C. P. Lai, T. T. Lu, Y. Chen, *Nat. Nanotechnol.* **2019**, *14*, 1160.
[34] N. Lyu, Z. Du, H. Qiu, P. Gao, Q. Yao, K. Xiong, Q. Tu, X. Li, B. Chen, M. Wang, G. Pan, N. Huang, Z. Yang, *Adv. Sci.* **2020**, *7*, 2002330.
[35] M. Qian, Q. Liu, Y. Wei, Z. Guo, Q. Zhao, *Bioact. Mater.* **2021**, *6*, 1464.
[36] J.-H. Yan, W. Meng, H. Shan, X.-P. Zhang, L.-M. Zou, L.-L. Wang, J.-S. Shi, X.-Y. Kong, *ACS Appl. Nano Mater.* **2021**, *4*, 1351.
[37] T. Luo, D. Wang, L. Liu, Y. Zhang, C. Han, Y. Xie, Y. Liu, J. Liang, G. Qiu, H. Li, D. Su, J. Liu, K. Zhang, *Adv. Sci.* **2021**, *8*, 2101065.
[38] Y. Ma, S. Gou, Z. Zhu, J. Sun, M. A. Shahbazi, T. Si, C. Xu, J. Ru, X. Shi, R. L. Reis, S. C. Kundu, B. Ke, G. Nie, B. Xiao, *Adv. Mater.* **2024**, https://doi.org/10.1002/adma.202309516.
[39] S. Wang, Y. Tian, W. Tian, J. Sun, S. Zhao, Y. Liu, C. Wang, Y. Tang, X. Ma, Z. Teng, G. Lu, *ACS Nano* **2016**, *10*, 8578.
[40] W. H. Chen, G. F. Luo, Q. Lei, S. Hong, W. X. Qiu, L. H. Liu, S. X. Cheng, X. Z. Zhang, *ACS Nano* **2017**, *11*, 1419.
[41] Y. Zhao, B. Yi, J. Hu, D. Zhang, G. Li, Y. Lu, Q. Zhou, *Adv. Funct. Mater.* **2023**, *33*, 2300710.
[42] Y. Xu, S. Wang, Z. Chen, R. Hu, Y. Zhao, K. Wang, J. Qu, L. Liu, *Biomaterials* **2021**, *276*, 121017.
[43] Z. Wang, N. Yang, Y. Hou, Y. Li, C. Yin, E. Yang, H. Cao, G. Hu, J. Xue, J. Yang, Z. Liao, W. Wang, D. Sun, C. Fan, L. Zheng, *Adv. Sci.* **2023**, *10*, 2302123.
[44] Y. Chen, T. Xiong, X. Zhao, J. Du, W. Sun, J. Fan, X. Peng, *Adv. Healthcare Mater.* **2023**, *12*, 2202085.
[45] H. Yu, A. Tiemuer, X. Yao, M. Zuo, H.-Y. Wang, Y. Liu, X. Chen, *Acta Pharm. Sin. B* **2023**, *14*, 378.
[46] S. Im, J. Lee, D. Park, A. Park, Y. M. Kim, W. J. Kim, *ACS Nano* **2019**, *13*, 476.
[47] G. Shu, W. Zhu, Y. Jiang, X. Li, J. Pan, X. Zhang, X. Zhang, S. K. Sun, *Adv. Funct. Mater.* **2021**, *31*, 2104472.
[48] R. Slovak, J. M. Ludwig, S. N. Gettinger, R. S. Herbst, H. S. Kim, *J. Immunother. Cancer* **2017**, *5*, 78.
[49] C. Yang, M. Wang, M. Chang, M. Yuan, W. Zhang, J. Tan, B. Ding, P. Ma, J. Lin, *J. Am. Chem. Soc.* **2023**, *145*, 7205.
[50] W. Jiang, W. Dong, M. Li, Z. Guo, Q. Wang, Y. Liu, Y. Bi, H. Zhou, Y. Wang, *ACS Nano* **2022**, *16*, 3881.
[51] B. Vander Lugt, A. A. Khan, J. A. Hackney, S. Agrawal, J. Lesch, M. Zhou, W. P. Lee, S. Park, M. Xu, J. DeVoss, C. J. Spooner, C. Chalouni, L. Delamarre, I. Mellman, H. Singh, *Nat. Immunol.* **2014**, *15*, 161.
[52] W. Li, J. X. Fan, D. W. Zheng, X. Z. Zhang, *Small* **2022**, *18*, 2205193.
[53] T. L. Boye, K. Maeda, W. Pezeshkian, S. L. Sonder, S. C. Haeger, V. Gerke, A. C. Simonsen, J. Nylandsted, *Nat. Commun.* **2017**, *8*, 1623.
[54] F. Fu, W. Wang, L. Wu, W. Wang, Z. Huang, Y. Huang, C. Wu, X. Pan, *ACS Nano* **2023**, *17*, 5486.
[55] Y. Jiang, K. Shao, F. Zhang, T. Wang, L. Han, X. Kong, J. Shi, *Aggregate* **2023**, *4*, 321.
[56] W. Bao, M. Liu, J. Meng, S. Liu, S. Wang, R. Jia, Y. Wang, G. Ma, W. Wei, Z. Tian, *Nat. Commun.* **2021**, *12*, 6399.
[57] L. Yang, H. Tang, X. Lin, Y. Wu, S. Zeng, Y. Pan, Y. Li, G. Xiang, Y. F. Lin, S. M. Zhuang, Z. Song, Y. Jiang, X. Liu, *Front. Cell Dev. Biol.* **2020**, *8*, 180.
[58] H. Lu, L. Hu, T. Li, S. Lahiri, C. Shen, M. S. Wason, D. Mukherjee, H. Xie, L. Yu, J. Zhao, *J. Biol. Chem.* **2012**, *287*, 43720.
[59] K. Wang, J. Li, Y. Yi, B. Lv, Y. Wu, C. Wang, H. Li, Y. Li, Y. Liu, X. Cai, X. Meng, X. Jiang, X. Zheng, Z. Zhou, W. Bu, *Nano Today* **2022**, *42*, 101355.
[60] Y. Huang, Y. Chen, S. Zhou, L. Chen, J. Wang, Y. Pei, M. Xu, J. Feng, T. Jiang, K. Liang, S. Liu, Q. Song, G. Jiang, X. Gu, Q. Zhang, X. Gao, J. Chen, *Nat. Commun.* **2020**, *11*, 622.
[61] C. Wang, H. Wang, H. Yang, C. Xu, Q. Wang, Z. Li, Z. Zhang, J. Guan, X. Yu, X. Yang, X. Yang, Z. Li, *Nano Res.* **2023**, *16*, 7323.

© 2024 Wiley-VCH GmbH

16163028, 0, Downloaded from https://onlinelibrary.wiley.com/doi/10.1002/adfm.202315551 by Universidade Do Minho, Wiley Online Library on [26/03/2024]. See the Terms and Conditions (https://onlinelibrary.wiley.com/terms-and-conditions) on Wiley Online Library for rules of use; OA articles are governed by the applicable Creative Commons License